Nanoscale

PAPER

Cite this: *Nanoscale*, 2022, **14**, 11703

Fluoride-free synthesis of anodic TiO_2 nanotube layers: a promising environmentally friendly method for efficient photocatalysts†

Muhammad Bilal Hanif, [a] Guru Karthikeyan Thirunavukkarasu, [a] Viktoriia Liapun,[a] Hryhorii Makarov,[b] Maros Gregor,[b] Tomas Roch,[b] Tomas Plecenik,[b] Karol Hensel,[c] Marcel Sihor, [d] Olivier Monfort [a] and Martin Motola *[a]

Received 20th June 2022,
Accepted 19th July 2022

DOI: 10.1039/d2nr03379h

rsc.li/nanoscale

TiO_2 nanotube (TNT) layers are generally prepared in fluoride-based electrolytes *via* electrochemical anodization that relies on the field-assisted dissolution of Ti metal forming nanoporous/nanotubular structures. However, the usage of fluoride ions is considered hazardous to the environment. Therefore, we present an environmentally friendly synthesis and application of TNT layers prepared in fluoride-free nitrate-based electrolytes. A well-defined nanotubular structure with thickness up to 1.5 μm and an inner tube diameter of ~55 nm was obtained within 5 min using aqueous $X(NO_3)_Y$ electrolytes ($X = Na^+$, K^+, Sr^{2+}, Ag^+). For the first time, we show the photocatalytic performance (using a model organic pollutant), $HO^•$ radical production, and thorough characterization of TNT layers prepared in such electrolytes. The highest degradation efficiency (k = 0.0113 min^{-1}) and $HO^•$ radical production rate were obtained using TNT layers prepared in $AgNO_3$ (Ag-NT). The intrinsic properties of Ag-NT such as the valence band maximum of ~2.9 eV, surface roughness of ~6 nm, and suitable morphological features and crystal structure were obtained. These results have the potential to pave the way for a more environmentally friendly synthesis of anodic TNT layers in the future using the next generation of fluoride-free nitrate-based electrolytes.

Introduction

The synthesis of TiO_2 nanotube (TNT) layers *via* anodization was first reported in 1984.[1] This discovery was initially overlooked, but after pioneering works conducted in 2005–2007,[2–4] anodic TNT layers have received significant attention. Indeed, due to their unique 1D morphology and exceptional physicochemical properties,[5–8] TNT layers are nowadays used in various applications including photocatalysis,[9] solar cells,[10] and biomedicine.[11] Anodic TNT layers can be grown directly from Ti substrate in suitable aqueous- or organic-based electrolytes.[2,12] In the last two decades, a plethora of different Ti substrates have been used as a starting material for TNT preparation including Ti foil,[4] Ti mesh,[13] Ti spheres,[14] Ti wires,[15] Ti alloys,[16–18] deposited Ti on Si, ITO,[20] FTO,[21] and electrodeposited Ti on Ni.[22] In most of the currently popular electrolytes, fluoride ions[5] (or halogen ions in general, such as chloride[23,24] and bromide[24]) are considered necessary to form the nanotubular structure in TNTs. The scientific community has generally adopted field-assisted dissolution supported by fluoride ions (so-called top-to-bottom synthesis) for TNT layer formation. Based on this theory, the following reactions (eqn (1)–(3)) occur in electrolytes containing fluoride ions:[5]

$$\text{Oxidation of Ti}: \quad Ti \rightarrow Ti^{4+} + 4e^- \tag{1}$$

$$\text{Formation of oxide layer}: \quad Ti^{4+} + 2H_2O \rightarrow TiO_2 + 4H^+ \tag{2}$$

$$\text{Dissolution of oxide layer}: \quad 4H^+ + F^- + TiO_2 \rightarrow [TiF_6]^2 + 2H_2O \tag{3}$$

Fluoride (or halogens in general) is considered an essential irreplaceable ingredient of the electrolyte for TNT layer synthesis. However, the replacement of fluoride ions would potentially provide: (i) less hazardous alternatives to highly toxic fluoride-containing compounds (*e.g.*, HF, NH_4F) and (ii)

[a]*Department of Inorganic Chemistry, Faculty of Natural Sciences, Comenius University Bratislava, Ilkovicova 6, 842 15 Bratislava, Slovakia. E-mail: martin.motola@uniba.sk; Tel: +421 2 9014 9374*
[b]*Department of Experimental Physics, Faculty of Mathematics, Physics, and Informatics, Comenius University Bratislava, 842 48 Bratislava, Slovakia*
[c]*Division of Environmental Physics, Faculty of Mathematics, Physics, and Informatics, Comenius University Bratislava, 842 48 Bratislava, Slovakia*
[d]*Institute of Environmental Technology, CEET, VSB-Technical University of Ostrava, 17. listopadu 15/2172, Ostrava-Poruba, Czech Republic*

†Electronic supplementary information (ESI) available: Summary of different parameters for TNT layer synthesis (table); representative SEM images of different TNT layers (figure); photocatalytic activity of TNT layers (figure); EDS analysis of TNT layers (figure); data from AFM (Table); Miller indices and position of diffractions (Table). See DOI: https://doi.org/10.1039/d2nr03379h

enhanced interfacial adhesion between the nanotubes and the underlying substrate. Indeed, TNT layers formed in fluoride-containing electrolytes are prone to peeling off from the underlying Ti substrate due to weak interfacial nanotube/substrate adhesion.[25] As alternatives, fluoride-free nitrate-based electrolytes (*e.g.*, $NaNO_3$, KNO_3, $AgNO_3$) seem promising. In fluoride-free electrolytes, the field-assisted dissolution by fluoride ions is not applicable. The second theory of nanotubular formation has been reported wherein the nanotubular structure forms around generated oxygen bubbles and relies on the viscous flow model, the oxygen bubble mold effect, and electronic current theory (so-called bottom-to-top synthesis).[26–30] To this day, there are only a few reports on TNT layers prepared in nitrate-based electrolytes[31–36] compared with the thousands of papers on TNT layers prepared in fluoride-containing ones. However, in some reports,[32] nitrates are added to fluoride-containing organic-based electrolytes to improve the morphological features of the TNT layers. Thus, it is not considered as a fluoride-free electrolyte. So far, the successful formation of TNT layers in fluoride-free nitrate-based electrolytes has been obtained using NH_4NO_3,[33–35] $NaNO_3$,[36] KNO_3,[36] and $AgNO_3$.[31] $Sr(NO_3)_2$ is another potential nitrate-based electrolyte applicable for TNT layer synthesis. To the best of our knowledge, there is no report on anodic TNT layers prepared in $Sr(NO_3)_2$ electrolytes. Moreover, all the reports so far solely focus on optimizing the anodic conditions for the synthesis of TNT layers in fluoride-free nitrate-based electrolytes; however, no potential application of these materials (experimental or theoretical) is provided. Such TNT layers could be potentially applicable in photoelectrochemical applications (*e.g.* photocatalysis) similar to their sister material, *i.e.*, TNT layers prepared in aqueous- or organic-based fluoride-containing electrolytes. Thus, the present study fills this knowledge gap, which is, as we believe, of high scientific interest.

In the present work, TNT layers were prepared *via* anodization in fluoride-free nitrate-based electrolytes, *i.e.*, $NaNO_3$, KNO_3, $Sr(NO_3)_2$, and $AgNO_3$. A thorough optimization of the anodization conditions was conducted for all electrolytes to obtain the most promising set of TNT layers (*i.e.*, with appropriate morphological features) for the photocatalytic degradation of a model organic pollutant. Although an organic dye is used (methylene blue), it is an excellent probe to evaluate the potential application of such TNT layers in environmental photocatalysis. The TNT layers were thoroughly characterized using scanning electron microscopy (SEM), energy-dispersive X-ray spectroscopy (EDS), X-ray diffraction (XRD), X-ray photoelectron spectroscopy (XPS), and ultraviolet photoelectron spectroscopy (UPS).

Experimental section

Synthesis of TNT layers

Titanium foil (Sigma Aldrich, Slovakia, 0.127 mm thick, 99.7% purity) was used as a starting substrate for the synthesis of TNT layers *via* anodization. Prior to anodization, the Ti foil was degreased by sonication in acetone (Central Chem, Slovakia) and isopropanol (Central Chem, Slovakia) for 10 min each. Firstly, the anodization conditions were optimized. All anodizations were conducted using a DC power supply (ET systems GmbH, Poland) at different applied potentials, anodization times, and current. A two-electrode configuration using graphite (3 cm^2, Chenjianqing, China) or titanium (3 cm^2, Sigma Aldrich, Slovakia, 0.127 mm thick, 99.7% purity) as a counter electrode and titanium foil (3 cm^2) as a working electrode was used. The distance between the electrodes was 1.5 cm. The electrolyte contained 1 g $X(NO_3)_Y$ (X = Na^+, K^+, Sr^{2+}, Ag^+; Acros Organics, Slovakia) and 200 mL distilled water (DIW, aqueous-based electrolyte) or 200 mL ethylene glycol (organic-based electrolyte). A full list of all the used electrolytes, their recipes, and anodization conditions is summarized in the ESI (Table S1†). After anodization, the as-prepared TNT layers were sonicated in isopropanol for approx. 5 s and dried by an air blower. Subsequently, the as-prepared TNT layers were annealed at 450 °C for 2 h (2 °C min^{-1}) in air to obtain crystalline TiO_2 (Fig. 1). The most promising TNT layers and their derivatives obtained for each nitrate-based electrolyte were prepared using the following: (i) Na-NT (1 g $NaNO_3$, 200 mL DIW, 30 V, 2 min, 0.8 A, graphite electrode), (ii) K-NT (1 g KNO_3, 200 mL DIW, 60 V, 2 min, 1 A, graphite electrode), (iii) Sr-NT (1 g $Sr(NO_3)_2$, 200 mL DIW, 30 V, 5 min, 1 A, graphite electrode), and (iv) Ag-NT (1 g $AgNO_3$, 200 mL DIW, 60 V, 1 min, 1 A, graphite electrode). These four TNT layers were further studied in more detail in the present work.

Characterization

The morphology, structure, surface roughness, and composition of the TNT layers were studied using: (i) scanning electron microscopy (SEM, Lyra 3 Tescan, at 10 kV) equipped with energy-dispersive X-ray spectroscopy (EDS), (ii) X-ray diffractometry in the grazing incidence mode (GI-XRD, PANalytical, Cu Kα radiation, λ = 1.5418 Å), (iii) atomic force microscopy (AFM, NT-MDT, NTegra Aura) in the semi-contact tapping mode using standard silicon AFM probes (NT-MDT, HA-NC ETALON series), (iv) X-ray photoelectron spectroscopy (XPS, Omicron multi-probe system with a hemispherical analyser) using monochromatic Al Kα X-rays (1486.6 eV), and (v) ultraviolet photoelectron spectroscopy (UPS, Omicron multi-probe system with a hemispherical analyser) with UV photon energy He(*I*) = 21.2 eV.

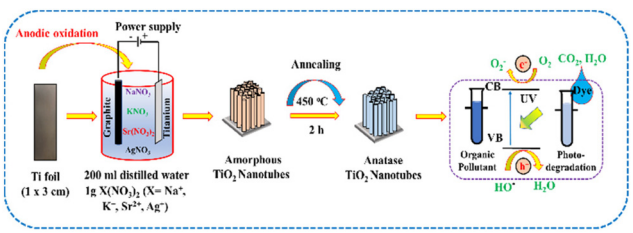

Fig. 1 Schematic illustration of the fabrication of TNT layers (Na-NT, K-NT, Sr-NT, and Ag-NT) in aqueous $X(NO_3)_Y$-based electrolytes (X = Na^+, K^+, Sr^{2+}, Ag^+) and the mechanism of MB photocatalytic degradation.

Fluorescence spectrophotometry (RF-6000, Shimadzu) was used to determine the amount of photogenerated hydroxyl radicals ($HO^{\bullet}$) under UVA (2 h irradiation) in a solution containing TNT layers and 0.5 mM coumarin (12 mL). Briefly, 0.3 mL of the solution was sampled out (20 min and 30 min step), and in the presence of $HO^{\bullet}$, coumarin formed hydroxycoumarin (fluorescent compound), which was detected at λ_{em} = 456 nm (λ_{ex} = 325 nm).[37] Standard curves were plotted with known concentrations of hydroxycoumarin (99+%, Alfa Aesar, Central Chem, Slovakia) to quantify the amount of generated $HO^{\bullet}$ under UVA irradiation. The experiments were repeated three times with the error not exceeding ±5%.

Photocatalytic activity

The photocatalytic degradation of methylene blue (MB, 10^{-5} M, Acros Organics, Slovakia) was evaluated under UVA irradiation (HQI TS-OSRAM 400 W, 1.3 mW cm^{-2} in the wavelength range of 335–380 nm). Prior to the photocatalytic measurements, TNT layers were immersed in MB solution (in the dark for 60 min) to achieve adsorption/desorption equilibrium and subsequently irradiated for 2 h. Every 20 min, the solution was sampled out and the decrease in MB absorbance (at λ_{max} = 660 nm) was monitored by a UV–VIS spectrophotometer (Jasco V-530). To confirm the stability of the samples, all photocatalytic measurements were repeated three times. Overall, the performance did not exceed ±5%, which confirms the good stability of the material.

Results and discussion

At first, the anodization conditions were optimized using all nitrate-based electrolytes to obtain TNT layers with the most promising morphological features. The optimization of different parameters was conducted, including: (i) counter electrode type (titanium *vs.* graphite), (ii) electrolyte type (aqueous- *vs.* organic-based), and (iii) anodization conditions (applied potential, anodization time). The results are summarized in the ESI (Table S1 and Fig. S1†). Subsequently, the photocatalytic properties of the most promising TNT layers, *i.e.*, those with well-defined nanotubular structures, were evaluated (Fig. S2†). Based on these preliminary results, we further studied in more detail the four TNT layers prepared in $NaNO_3$ (Na-NT), KNO_3 (K-NT), $Sr(NO_3)_2$ (Sr-NT), and $AgNO_3$ (Ag-NT) that possess the best morphological features, where the whole anodized surface area was covered by well-defined nanotubes and showed the highest photocatalytic degradation efficiencies.

Thorough SEM characterization was conducted on different areas of the TNT layers to confirm the nanotubular structure over the whole anodized area. Representative top and cross-sectional SEM images are shown in Fig. 2. The morphological features are summarized in Table 1. Anodization led to the formation of 0.5–1.4 μm thick TNT layers with an inner tube diameter ranging from 15 nm to 55 nm in all the nitrate-based electrolytes. As previously reported,[38–40] TNT layers prepared in fluoride-containing electrolytes can be easily removed from the underlying Ti substrate by simple bending of the substrate, which results in nanotubes peeling off of the substrate. The reason for the poor interfacial adhesion is two-fold: (1) the anodization of Ti in fluoride-containing electrolytes inherently leads to the formation of a fluoride-rich layer at the nanotube/substrate interface, which decreases the adhesion,[41,42] and (2) residual stress (effect of growth and chemical dissolution stress) at the nanotube/substrate interface leads to poor adhesion.[25,43] These inherent issues can be partially overcome by adjusting the anodization process, *i.e.*, using fluoride-free electrolytes. Although residual stress is still present during anodization in all electrolytes in general, the formation of nanotubes in fluoride-free (*e.g.*, nitrate-based) electrolytes eliminates the poor adhesion, which is not present in such electrolytes. The interfacial nanotube/substrate adhesion of the present TNT layers was evaluated *via* a simple mechanical bending test. When bending Na-NT, K-NT, Sr-NT, and Ag-NT,

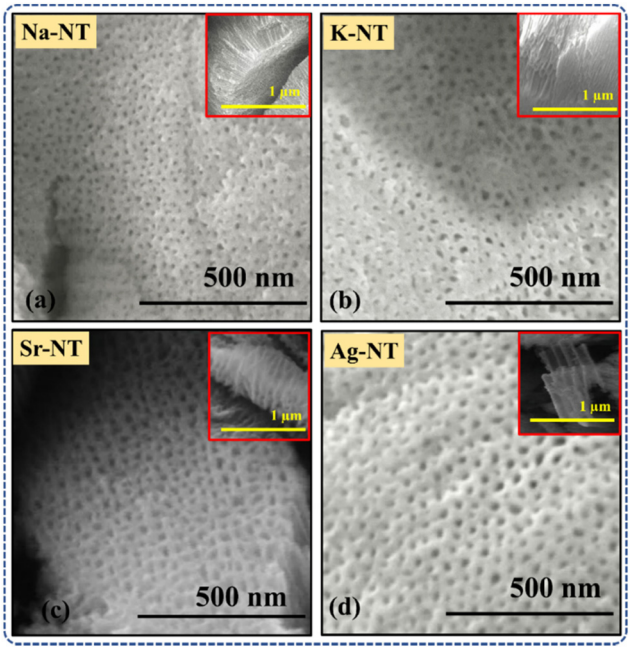

Fig. 2 Representative top and cross-sectional (insets) SEM images of TNT layers prepared in (a) $NaNO_3$ (Na-NT), (b) KNO_3 (K-NT), (c) $Sr(NO_3)_2$ (Sr-NT), and (d) $AgNO_3$ (Ag-NT).

Table 1 Morphological features and root mean square values of the TNT layers prepared in $NaNO_3$ (Na-NT), KNO_3 (K-NT), $Sr(NO_3)_2$ (Sr-NT), and $AgNO_3$ (Ag-NT)

	Morphological features			
Sample	Tube diameter (nm)	Tube wall thickness (nm)	Layer thickness (μm)	S_q (nm)
Na-NT	15–25	15–25	0.7–1.1	55.5
K-NT	20–30	10–20	0.5–1.4	81.8
Sr-NT	30–40	15–25	0.5–0.9	27.0
Ag-NT	45–55	10–20	0.7–0.9	6.4

no nanotubes were peeled off due to the absence of the fluoride-rich layer. Thus, a good nanotube/substrate interfacial adhesion was observed.

During anodization, cations present in the electrolyte (Na^+, K^+, Sr^{2+}, Ag^+) might deposit on the surface of the formed TiO_2 nanotubes or incorporate into the TiO_2 structure as neutral elements and/or their oxides. EDS analysis was conducted to evaluate the amount of elements present in Na-NT, K-NT, Sr-NT, and Ag-NT, and the results are summarized in the ESI (Fig. S3†). Briefly, 0.07 wt% (0.05 at%) K and 0.49 wt% (0.13 at%) Ag were detected in K-NT and Ag-NT, respectively. No Na and Sr were detected by EDS in Na-NT and Sr-NT, respectively.

Moreover, XPS was conducted to determine the chemical states and the elemental compositions of the TNT layers. Fig. 3a–d shows the XPS spectra of Na-NT, K-NT, Sr-NT, and Ag-NT. All the TNT layers showed the presence of Ti 2p, O 1s and C 1s at approx. 469 eV, 530 eV, and 285 eV, respectively. The Ti 2p peaks found in the TNT layers are assigned to the Ti^{4+} oxidation state and the carbon C 1s to surface contamination. Interestingly, only in Ag-NT, a minor concentration of Ag was detected at approx. 369 eV, corresponding to Ag 3d (Ag $3d_{3/2}$ and Ag $3d_{3/5}$). However, peaks of Na, K, and Sr were not detected in the XPS spectra of Na-NT, K-NT, and Sr-NT, respectively, due to the detection limit of XPS. Finally, the valence band maxima (VBM) of Na-NT, K-NT, Sr-NT, and Ag-NT were determined to be approx. 3.02 eV, 3.03 eV, 3.28 eV, and 2.9 eV, respectively (Fig. 3e). Interestingly, due to the detectable presence of Ag and K (Fig. 3d, and EDS, Fig. S3†), lower VBM were observed for Ag-NT and K-NT compared to those for Na-NT and Sr-NT. This lowering in VBM can potentially enhance the utilization of the incident light.[44,45]

Additional information on the surface morphology alterations of Na-NT, K-NT, Sr-NT, and Ag-NT was acquired by AFM (Fig. 4). The nanoscale roughness was determined on a 1 × 1 μm^2 area, and the complete data are summarized in the ESI (Table S2†). The overall root mean square values (S_q in nm, Table 1) differed for each particular TNT layer, and follow the order of K-NT ($S_q \sim 82$ nm) > Na-NT ($S_q \sim 56$ nm) > Sr-NT ($S_q \sim 27$ nm) > Ag-NT ($S_q \sim 6$ nm). The difference in the surface roughness is explained as follows. The range of TNT layer thickness (Table 1) is a crucial factor for the overall surface roughness. Indeed, the highest S_q was obtained for K-NT, where the thickness of the layer is in the range of 0.5 μm to 1.4 μm. Due to this relatively large thickness range, the surface of K-NT is ripple-like; thus, the highest S_q was obtained. As the difference in thickness range decreased, the overall S_q also decreased, as seen in Table 1. Indeed, in the case of Ag-NT, the surface is relatively smooth with $S_q \sim 6$ nm. In Ag-NT, the length of the tubes (overall thickness of the layer) is almost similar over the whole anodized area, and the difference did not exceed ±0.1 μm. Thus, a rather smooth surface was obtained in Ag-NT compared to a rather rough one in the case of K-NT.

Fig. 5 shows the XRD patterns of annealed Na-NT, K-NT, Sr-NT, and Ag-NT. Three different phases were identified in the four types of TNT layers: tetragonal anatase TiO_2 ($P4_2/mnm$; ICCD 01-086-1157),[13,46] tetragonal rutile TiO_2 ($I4_1/amd$; ICCD 00-021-1276),[13,46] and hexagonal metallic Ti ($P6_3/mmc$; ICCD 00-044-1294).[13,46] The diffractions are attributed to the follow-

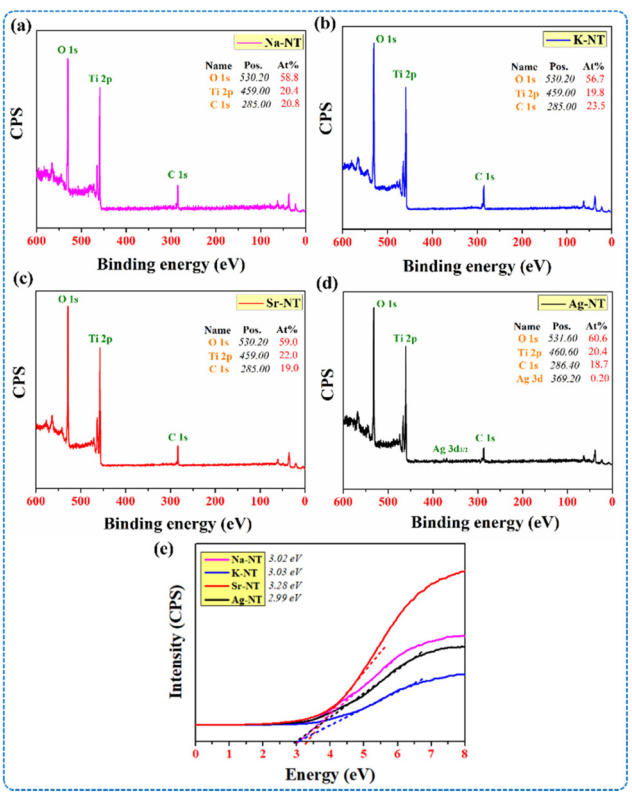

Fig. 3 XPS spectra of the TNT layers prepared in (a) $NaNO_3$ (Na-NT), (b) KNO_3 (K-NT), (c) $Sr(NO_3)_2$ (Sr-NT), and (d) $AgNO_3$ (Ag-NT). (e) Kubelka–Munk curves from ultraviolet photoelectron spectroscopy (UPS).

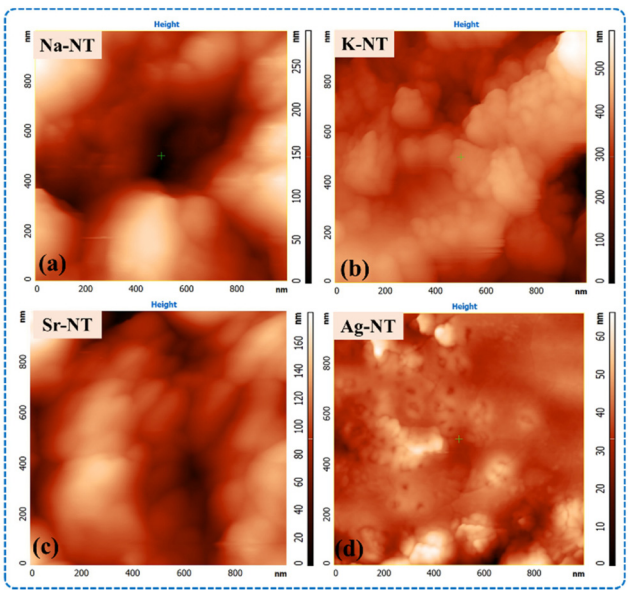

Fig. 4 AFM topography images of the TNT layers prepared in (a) $NaNO_3$ (Na-NT), (b) KNO_3 (K-NT), (c) $Sr(NO_3)_2$ (Sr-NT), and (d) $AgNO_3$ (Ag-NT).

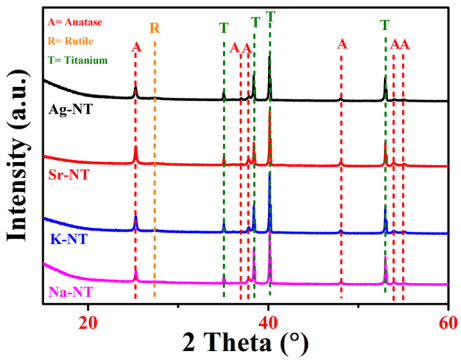

Fig. 5 XRD patterns of the TNT layers prepared in (a) $NaNO_3$ (Na-NT), (b) KNO_3 (K-NT), (c) $Sr(NO_3)_2$ (Sr-NT), and (d) $AgNO_3$ (Ag-NT) annealed at 450 °C in air. A – anatase TiO_2; R – rutile TiO_2; T – metallic Ti.

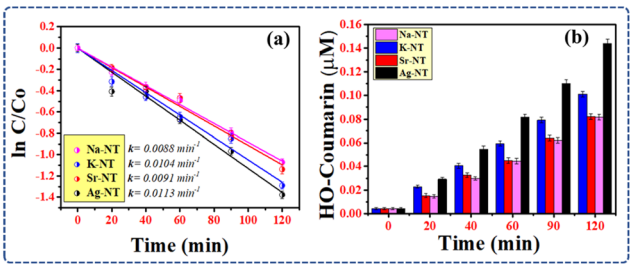

Fig. 6 (a) Photocatalytic degradation of MB and (b) formation of HO$^{\bullet}$ radicals by coumarin assay using different the TNT layers prepared in $NaNO_3$ (Na-NT), KNO_3 (K-NT), $Sr(NO_3)_2$ (Sr-NT), and $AgNO_3$ (Ag-NT).

ing: (i) the as-prepared amorphous TNT layers undergo amorphous-to-crystalline transformation at 450 °C to form anatase TiO_2; (ii) as reported,[47–49] rutile TiO_2 stems from a thermal oxide layer present between the nanotube layer and the underlying Ti substrate formed during thermal treatment; and (iii) metallic Ti diffractions stems from the underlying Ti substrate.[19,47] The diffraction positions, Miller indices, and calculated crystallite sizes (of the (101) anatase TiO_2 diffraction at approx. 2θ = 25.3°) are summarized in the ESI (Tables S3 and S4†). The XRD patterns of the present TNT layers prepared in fluoride-free nitrate-based electrolytes are similar to those of TNT layers prepared in fluoride-containing ones.[47] Indeed, the TNTs prepared in the nitrate-based electrolytes possess similar morphological (SEM, Fig. 2), surface (AFM, Fig. 4), and structural properties (XRD, Fig. 5) as TNTs prepared in fluoride-containing electrolytes,[5] without the use of hazardous compounds containing fluorides (*e.g.*, HF, NH_4F) during anodization. Moreover, a significantly lower anodization time is needed to obtain a well-defined nanotubular structure using nitrate-based electrolytes (1–5 min) compared to TNT layers prepared in the currently popular fluoride-containing organic-based electrolytes (1–4 h).[2–8] Thus the preparation of TNT layers in nitrate-based electrolytes seems promising as it is economically and environmentally friendly.

Finally, concerning the photocatalytic degradation of MB under UVA irradiation in the presence of Na-NT, K-NT, Sr-NT, and Ag-NT, the corresponding degradation rates are summarized in Fig. 6a. In general, the photocatalytic degradation of an organic dye follows a first-order reaction.[9] The highest photocatalytic degradation rate was obtained for Ag-NT (k = 0.0113 min^{-1}), followed by K-NT (k = 0.0104 min^{-1}), Sr-NT (k = 0.0091 min^{-1}), and Na-NT (k = 0.0088 min^{-1}). Several factors affect the overall photocatalytic degradation rate of a material, *e.g.*, textural properties, structure (phase and elemental) composition, and surface area. It is worth noting that we do not discuss the potential sensitization of the TNT layers by MB, since the main goal of the present study is to highlight the promising applicability of TNT layers prepared in fluoride-free nitrate-based electrolytes. In the case of Ag-NT, the interplay of the structure, morphology, and composition led to the most efficient degradation of MB. Based on SEM (Fig. 2 and Table 1), the nanotubes with the largest diameter were obtained in Ag-NT compared to the other materials. Indeed, this increases the number of active sites available on the surface of Ag-NT, so the pollutant can be better adsorbed and subsequently degraded. Moreover, during the anodization of Ti in $AgNO_3$, Ag present in the electrolyte was deposited on the nanotube walls, as confirmed by EDS (0.13 at% Ag; Fig. S3†) and XPS (0.20% Ag; Fig. 3d), in the form of an oxide (Ag_2O) or metallic Ag. The decoration of TiO_2 by Ag enhances the overall photocatalytic efficiency.[44,45] This is due to the intimate contact between TiO_2 and Ag_2O, which results in a semiconductor–metal heterojunction (S–M heterojunction) structure with favourable positions of the conduction (CB) and valence bands (VB) in the energy diagram. Indeed, the photogenerated electrons accumulated in the CB of Ag_2O are transferred to the CB of TiO_2 since it has a more positive CB compared to that of Ag_2O. Similarly, the photogenerated holes accumulated in the VB of TiO_2 are captured within the VB of Ag_2O. Such a heterojunction limits the recombination of the charge carriers (electrons and holes), thus enhancing the photocatalytic activity of Ag-NT. In the case of metallic Ag, the enhanced photocatalytic activity is due to the intimate contact between TiO_2 and Ag. Indeed, the photogenerated electrons are accumulated in Ag, which plays the role of an electron trap, thus leading to enhanced separation of the charge carriers (e^- and h^+), where the holes can efficiently produce hydroxyl radicals. The photogenerated charge carriers react with H_2O, OH^-, and O_2 adsorbed on the surface of Ag-NT to form HO$^{\bullet}$ and $O_2^{\bullet-}$ that subsequently decompose organic pollutants to CO_2 and H_2O. In particular, HO$^{\bullet}$ is responsible for organic pollutants being degraded. Indeed, the amount of generated HO$^{\bullet}$ is a crucial factor to obtain high degradation efficiencies. The production of HO$^{\bullet}$ proceeds at the material surface induced by incident light and depends primarily on the material's surface area and composition. To support the bold statements regarding the photocatalytic degradation efficiency using Ag-NT (and the other prepared nanotubes), the HO$^{\bullet}$ radical production was evaluated, and the results are shown in Fig. 6b. The highest HO$^{\bullet}$ production was obtained in Ag-NT, followed by K-NT and Sr-NT/Na-NT. The trend of HO$^{\bullet}$ production is similar

to that of the photocatalytic degradation rate; thus, the obtained data are in good agreement. Considering all the present results, the interplay of structure, morphology, composition, and $HO^{\bullet}$ production is in favour of Ag-NT. All in all, we present a less hazardous and more environmentally and economically friendly synthesis of anodic TiO_2 nanotube layers using fluoride-free electrolytes based on nitrates. A well-defined nanotubular structure was obtained within 5 min, and the formed NTs seem promising for photoelectrochemical and photochemical applications, including solar photocatalysis for environmental remediation.

Conclusions

TNT layers were prepared *via* anodization in fluoride-free the nitrate-based electrolytes $NaNO_3$, KNO_3, $Sr(NO_3)_2$, and $AgNO_3$. Thorough optimization of the anodization parameters, including the applied potential, anodization time, and counter electrode type, was conducted. The optimized anodization led to the formation of 0.5–1.5 μm thick TNT layers with an inner tube diameter ranging from 15 nm to 55 nm in all the nitrate-based electrolytes with good adhesion to the underlying Ti substrate. The smoothest TNT layers were obtained in $AgNO_3$ (Ag-NT) with a surface roughness of $S_q \sim 6$ nm. The highest photocatalytic degradation rate of MB was obtained using Ag-NT ($k = 0.0113\ min^{-1}$). This is due to the interplay of the structure, morphology, and composition of Ag-NT. The present results show how promising the synthesis of anodic TNT layers is in fluoride-free nitrate-based electrolytes, which is less hazardous due to the absence of fluoride and more economical due to the lowering of the anodization time to a few minutes. These results can pave the way for a more environmentally friendly synthesis of anodic TNT layers in the future using the next generation of nitrate-based electrolytes.

Author contributions

The manuscript was written through contributions of all authors. All authors have given their approval to the final version of the manuscript. Muhammad Bilal Hanif: writing, investigation, visualization, methodology, reviewing, editing. Guru Karthikeyan Thirunavukkarasu: writing, investigation, visualization, methodology, reviewing, editing. Viktoriia Liapun: writing, investigation, visualization, methodology, reviewing, editing. Hryhorii Makarov: investigation, methodology. Maros Gregor: investigation, methodology. Tomas Roch: investigation, methodology. Tomas Plecenik: investigation, methodology, funding acquisition. Karol Hensel: investigation, methodology, editing, reviewing. Marcel Sihor: investigation, methodology, editing, reviewing. Olivier Monfort: editing, reviewing, writing, funding acquisition. Martin Motola: supervision, conceptualization, writing, reviewing, editing, visualization, funding acquisition.

Conflicts of interest

There are no conflicts to declare.

Acknowledgements

This work has been partially supported by the project USCCCORD (ŽoNFP: NFP313020BUZ3), co-financed by the European Regional Development Fund within the Operational Programme Integrated Infrastructure. This work was also supported by (i) Grant of the Comenius University Bratislava for Young Scientists: UK/3/2022, (ii) Slovak Research and Development Agency (APVV): APVV-21-0039, APVV-20-0566, and APVV-21-0053, and (iii) Scientific Grant Agency of the Slovak Ministry of Education, Sciences, Research and Sport (VEGA): 1/0062/22. We acknowledge ERDF "Institute of Environmental Technology – Excellent Research" (No. CZ.02.1.01/0.0/0.0/16_019/0000853) for their support and by using Large Research Infrastructure ENREGAT supported by the Ministry of Education, Youth and Sports of the Czech Republic under project No. LM2018098.

Notes and references

1 M. Assefpour-Dezfuly, C. Vlachos and E. H. Andrews, *J. Mater. Sci.*, 1984, **19**, 3626–3639.
2 J. M. MacAk, K. Sirotna and P. Schmuki, *Electrochim. Acta*, 2005, **50**, 3679–3684.
3 J. M. Macak, H. Tsuchiya, A. Ghicov, K. Yasuda, R. Hahn, S. Bauer and P. Schmuki, *Curr. Opin. Solid State Mater. Sci.*, 2007, **11**, 3–18.
4 S. P. Albu, A. Ghicov, J. M. Macak and P. Schmuki, *Phys. Status Solidi RRL*, 2007, **1**, R65–R67.
5 K. Lee, A. Mazare and P. Schmuki, *Chem. Rev.*, 2014, **114**, 9385–9454.
6 D. Regonini, G. Chen, C. Leach and F. J. Clemens, *Electrochim. Acta*, 2016, **213**, 31–36.
7 J. M. Macák, H. Tsuchiya, A. Ghicov and P. Schmuki, *Electrochem. Commun.*, 2005, **7**, 1133–1137.
8 R. Beranek, H. Tsuchiya, T. Sugishima, J. M. Macak, L. Taveira, S. Fujimoto, H. Kisch and P. Schmuki, *Appl. Phys. Lett.*, 2005, **87**, 243114.
9 J. M. Macak, M. Zlamal, J. Krysa and P. Schmuki, *Small*, 2007, **3**, 300–304.
10 P. Roy, D. Kim, K. Lee, E. Spiecker and P. Schmuki, *Nanoscale*, 2010, **2**, 45–59.
11 M. Motola, J. Capek, R. Zazpe, J. Bacova, L. Hromádko, L. Bruckova, S. Ng, J. Handl, Z. Spotz, P. Knotek, K. Baishya, P. Majtnerova, J. Prikryl, H. Sopha, T. Rousar and J. M. Macak, *ACS Appl. Bio Mater.*, 2020, **3**, 6447–6456.
12 J. M. Macak, H. Tsuchiya, L. Taveira, S. Aldabergerova, P. Schmuki, S. Aldabergerova and P. Schmuki, *Angew. Chem., Int. Ed.*, 2005, **44**, 7463–7465.

13 M. Motola, L. Satrapinskyy, T. Roch, J. Šubrt, J. Kupčík, M. Klementová, M. Jakubičková, F. Peterka and G. Plesch, *Catal. Today*, 2017, **287**, 59–64.

14 H. Sopha, L. Hromadko, M. Motola and J. M. Macak, *Electrochem. Commun.*, 2020, **111**, 106669.

15 Z. Liu and M. Misra, *ACS Nano*, 2010, **4**, 2196–2200.

16 A. L. Escada, R. Z. Nakazato and A. P. R. A. Claro, *Mater. Res.*, 2017, **20**, 1282–1290.

17 J. M. Macak, H. Tsuchiya, L. Taveira, A. Ghicov and P. Schmuki, *J. Biomed. Mater. Res., Part A*, 2005, **75**, 928–933.

18 S. Hejazi, M. Altomare, N. T. Nguyen, S. Mohajernia, M. Lickleder and P. Schmuki, *Appl. Mater. Today*, 2019, **14**, 118–125.

19 M. Motola, E. Dworniczek, L. Satrapinskyy, G. Chodaczek, J. Grzesiak, M. Gregor, T. Plecenik, J. Nowicka and G. Plesch, *Chem. Pap.*, 2019, **73**, 1163–1172.

20 T. H. Meen, B. G. Fu, Y. C. Chen, W. R. Chen, Y. W. Chen and C. J. Huang, *IEEE Conf. Electron Devices Solid-State Circuits 2007, EDSSC*, 2007, vol. 2007, pp. 621–623.

21 H. Kmentova, S. Kment, L. Wang, S. Pausova, T. Vaclavu, R. Kuzel, H. Han, Z. Hubicka, M. Zlamal, J. Olejnicek, M. Cada, J. Krysa and R. Zboril, *Catal. Today*, 2017, **287**, 130–136.

22 H. Sopha, Y. Norikawa, M. Motola, L. Hromadko, J. Rodriguez-Pereira, J. Cerny, T. Nohira, K. Yasuda and J. M. Macak, *Electrochem. Commun.*, 2020, **118**, 106788.

23 S. W. Ng, F. K. Yam, K. P. Beh and Z. Hassan, *Sains Malays.*, 2014, **43**, 947–951.

24 Q. A. Nguyen, Y. V. Bhargava and T. M. Devine, *Electrochem. Commun.*, 2008, **10**, 471–475.

25 S. Cao, W. Huang, L. Wu, M. Tian and Y. Song, *Langmuir*, 2018, **34**, 13888–13896.

26 J. M. Albella, I. Montero and J. M. Martinez-Duart, *Electrochim. Acta*, 1987, **32**, 255–258.

27 X. Zhu, L. Liu, Y. Song, H. Jia, H. Yu, X. Xiao and X. Yang, *Monatshefte für Chemie - Chemical Monthly*, 2008, **139**, 999–1003.

28 X. F. Zhu, Y. Song, L. Liu, C. Y. Wang, J. Zheng, H. B. Jia and X. L. Wang, *Nanotechnology*, 2009, **20**, 475303.

29 J. E. Houser and K. R. Hebert, *Nat. Mater.*, 2009, **8**, 415–420.

30 S. J. Garcia-Vergara, P. Skeldon, G. E. Thompson and H. Habazaki, *Electrochim. Acta*, 2006, **52**, 681–687.

31 N. Lu, J. Zhang, Y. Dan, M. Sun, T. Gong, X. Li and X. Zhu, *Electrochem. Commun.*, 2021, **126**, 107022.

32 A. Pancielejko, P. Mazierski, W. Lisowski, A. Zaleska-Medynska, K. Kosek and J. Łuczak, *ACS Sustainable Chem. Eng.*, 2018, **6**, 14510–14522.

33 E. Song, Y. T. Kim and J. Choi, *Electrochem. Commun.*, 2019, **109**, 106610.

34 K. Yamaguchi, Y. Funane and N. Ohtsu, *Surf. Coat. Technol.*, 2020, **387**, 125469.

35 N. Ohtsu, M. Bai and K. Yamaguchi, *Surf. Coat. Technol.*, 2019, **374**, 65–71.

36 R. Zhu, C. Li, P. Li, X. Shen, J. Chen, Y. Song and X. Zhu, *Electrochem. Commun.*, 2021, **129**, 107093.

37 A. Marion, M. Brigante and G. Mailhot, *Atmos. Environ.*, 2018, **195**, 179–186.

38 K. Villa, H. Sopha, J. Zelenka, M. Motola, L. Dekanovsky, D. C. Beketova, J. M. Macak, T. Ruml and M. Pumera, *Small*, 2022, 2106612.

39 D. Beketova, M. Motola, H. Sopha, J. Michalicka, V. Cicmancova, F. Dvorak, L. Hromadko, B. Frumarova, M. Stoica and J. M. Macak, *ACS Appl. Nano Mater.*, 2020, **3**, 1553–1563.

40 H. Michalkova, Z. Skubalova, H. Sopha, V. Strmiska, B. Tesarova, S. Dostalova, P. Svec, L. Hromadko, M. Motola, J. M. Macak, V. Adam and Z. Heger, *J. Hazard. Mater.*, 2020, **388**, 122054.

41 H. Habazaki, K. Fushimi, K. Shimizu, P. Skeldon and G. E. Thompson, *Electrochem. Commun.*, 2007, **9**, 1222–1227.

42 D. Yu, X. Zhu, Z. Xu, X. Zhong, Q. Gui, Y. Song, S. Zhang, X. Chen and D. Li, *ACS Appl. Mater. Interfaces*, 2014, **6**, 8001–8005.

43 H. M. Ouyang, G. T. Fei, Y. Zhang, H. Su, Z. Jin, S. H. Xu and L. De Zhang, *J. Mater. Chem. C*, 2013, **1**, 7498–7506.

44 L. Barrientos, P. Allende, M. Á. Laguna-Bercero, J. Pastrián, J. Rodriguez-Becerra and L. Cáceres-Jensen, *J. Phys. Chem. Solids*, 2018, **119**, 147–156.

45 K. Li, C. Teng, S. Wang and Q. Min, *Front. Chem.*, 2021, **9**, 15.

46 M. Motola, L. Satrapinskyy, M. Čaplovicová, T. Roch, M. Gregor, B. Grančič, J. Greguš, Ľ. Čaplovič and G. Plesch, *Appl. Surf. Sci.*, 2018, **434**, 1257–1265.

47 M. Motola, L. Hromadko, J. Prikryl, H. Sopha, M. Krbal and J. M. Macak, *Electrochim. Acta*, 2020, **352**, 136479.

48 S. P. Albu, H. Tsuchiya, S. Fujimoto and P. Schmuki, *Eur. J. Inorg. Chem.*, 2010, **2010**, 4351–4356.

49 S. Das, R. Zazpe, J. Prikryl, P. Knotek, M. Krbal, H. Sopha, V. Podzemna and J. M. Macak, *Electrochim. Acta*, 2016, **213**, 452–459.